Published in final edited form as:
Biochemistry. 2012 February 7; 51(5): 974–985. doi:10.1021/bi201135s.

The diheme cytochrome *c* peroxidase from *Shewanella oneidensis* requires reductive activation†

Gökçe Su Pulcu[a,‡], **Katherine E. Frato**[a,‡], **Rupal Gupta**[b], **Hao-Ru Hsu**[a], **George A. Levine**[a], **Michael P. Hendrich**[b], and **Sean J. Elliott**[a,*]

[a]Department of Chemistry, 590 Commonwealth Avenue, Boston University, Boston, MA 02215

[b]Department of Chemistry, Carnegie Mellon University, Pittsburg, PA 15213

Abstract

We report the characterization of the diheme cytochrome *c* peroxidase (C*c*P) from *Shewanella oneidensis* (*So*) using UV/Visible absorbance, Electron Paramagnetic Resonance Spectroscopy, and Michaelis-Menten kinetics. While sequence alignment with other bacterial diheme cytochrome *c* peroxidases suggests that *So* C*c*P may be active in the as-isolated state, we find that *So* C*c*P requires reductive activation for full activity, similar to the canonical *Pseudomonas*-type of bacterial C*c*P enzyme. Peroxide turnover initiated with oxidized *So* C*c*P shows a distinct lag-phase, which we interpret as reductive activation *in situ*. A simple kinetic model is sufficient to recapitulate the lag-phase behavior of the progress curves and separate the contributions of reductive activation and peroxide turnover. The rates of catalysis and activation differ between MBP-fusion and tag-free *So* C*c*P, and also depend on the identity of the electron donor. Combined with Michaelis-Menten analysis these data suggest that *So* C*c*P can accommodate electron donor binding in several possible orientations, and that the presence of the MBP tag affects the availability of certain binding sites. To further investigate the structural basis of reductive activation in *So* C*c*P we introduced mutations into two different regions of the protein that have been suggested to be important for reductive activation in homologous bacterial C*c*Ps. Mutations in a flexible loop region neighboring the low-potential heme significantly increased the activation rate, confirming the importance of flexible loop regions of the protein in converting the inactive, as-isolated enzyme into the activated form.

Reactive oxygen species such as hydrogen peroxide and superoxide are generated in hypoxic conditions as a result of a leaky or inefficient electron transport chain (1), which may further yield toxic hydroxyl radicals through Fenton chemistry (2). For many gram negative bacteria, it is thought that periplasmic peroxide scavenging is achieved by soluble diheme cytochrome *c* peroxidases (3). Bacterial diheme cytochrome *c* peroxidases (BC*c*Ps[1]) differ from the canonical monoheme peroxidases such as horseradish peroxidase (HRP) (4)

†This work was supported by a National Institutes of Health research grant (R01-GM072663), and the Boston University Undergraduate Research Opportunities Program.

Address correspondence to S.J.E. at Department of Chemistry, Boston University, 590 Commonwealth Ave. Boston, MA, 02215, tel. 1-617-358-2816, fax. 1-617-353-4446, elliott@bu.edu.
‡These authors contributed equally to the work.

Conflict of Interest Declaration. The authors declare no competing financial interest.

Supporting Information **Available.** Mutagenesis primers, Python code for least-squares fitting of lag-phase kinetics data and SDS-PAGE gel of *So* C*c*P purification as MBP-fusion. This information is available free of charge via the internet at http://pubs.acs.org.

[1]Abbreviations: C*c*P, cytochrome *c* peroxidase; BC*c*P, bacterial cytochrome *c* peroxidase; MBP, maltose binding protein; HRP, horseradish peroxidase; *Psa*, *Pseudomonas aeruginosa*; *So*, *Shewanella oneidensis*; *Gs*, *Geobacter sulfurreducens*; *Ne*, *Nitrosomonas europaea*; *Rc*,*Rhodobacter capsulatus*; *Pd*, *Paracoccus denitrificans*; *Pss*, *Pseudomonas stutzeri*; *Psn*, *Pseudomonas nautica*; *Mc*, *Methyloccocus casulatus* (Bath); NHE, Normal Hydrogen Electrode; EPR, Electron Paramagnetic Resonance; S-100, Sepharcryl 100.

and yeast cytochrome *c* peroxidase (*y*C*c*P) (5) in their cofactor content and mechanism. The two heme cofactors in bacterial peroxidase enzymes are covalently bound within two separate cytochrome *c*-like domains. In all characterized BC*c*Ps, the high-potential (~ +330 mV vs hydrogen) Met-His ligated heme ("H-heme") serves as an electron transfer site, while the other, low-potential 'L-heme' (around −300mV vs. NHE) serves as the peroxidatic active site (6, 7). In the as-isolated state of the BC*c*P, both heme sites are in the ferric oxidation state, with the H-heme in a low-spin/high-spin equilibrium and the L-heme in a low-spin state (7). The high-potential heme, which is not present in monoheme peroxidases, may store a second oxidizing equivalent during the catalytic cycle (6), and is hypothesized to mediate electron transfer from electron donor proteins to the peroxidatic heme (8, 9).

Most BC*c*Ps are isolated in a state that is catalytically inactive where both hemes are each in the ferric state, as exemplified by the diheme peroxidase from *Pseudomonas aeruginosa* (*Psa*) (10). In the absence of reducing equivalents provided by an electron donor protein or small molecule such as ascorbate, both hemes of the BC*c*P remain in the ferric state where the active site is bis-His ligated, preventing binding of the peroxide substrate (11), as illustrated in Figure 1. The active form of the enzyme can be achieved by a one-electron reduction termed 'reductive activation': reduction of the H-heme results in local conformational changes that cause reorientation of the liganding groups on the low-potential heme, allowing for peroxide to access the active site (Figure 1B, 11, 12, 13). The overall phenomenon of reductive activation may serve a regulatory role, preventing turnover of the peroxidase in the absence of sufficient reducing equivalents provided by periplasmic electron donor proteins.

The reductive activation process is an essential step in most of the known BC*c*Ps. In addition to the *Psa* enzyme (10), reductive activation is required for the BC*c*Ps from *Paracoccus denitrificans (Pd)* (14), *Pseudomonas nautica (Psn)* (15), *Rhodobacter capsulatus (Rc)* (16), *Pseudomonas stutzeri (Pss)* (17) and *Geobacter sulfurreducens (Gs)* (18). In contrast, diheme peroxidases from *Nitrosomonas europaea (Ne)* (19) and *Methyloccocus casulatus* (Bath) (20) do not need to undergo the activation step; the crystal structure of *Ne* C*c*P shows that the low-potential heme is pentacoordinate in the as-isolated form (13) (Figure 1B**, blue**). A sequence alignment of representative BC*c*P enzymes (Figure 2) shows that the sequences of key loop regions that change conformation during reductive activation differ between *Psa*-type C*c*Ps that require reductive activation and *Ne* C*c*P, which does not. Swapping only two amino acids in one of these loop regions in the *Psa*-type C*c*P from *Geobacter sulfurreducens* generates a constitutively active protein, mimicking the *Nitrosomonas*-like class of BC*c*Ps (18). Intriguingly, on the basis of sequence the *Shewanella oneidensis* (*So*) C*c*P is highly similar to *Ne* C*c*P (60% identity by primary amino acid sequence), and diverges more strongly from *Psa*-like C*c*Ps (44% identity to *Psa* C*c*P). The sequence similarities between *Ne* and *So* are particularly striking in the flexible loop regions that have been identified as mediators of the conformational changes in reductive activation. We sought to test the hypothesis that, based on sequence identity, the *So* C*c*P should be a member of the *Ne*-type functional sub-class of BC*c*Ps, which would not require reductive activation.

In this report, we characterize the peroxidase activity of a diheme peroxidase from *Shewanella oneidensis*. We express the *So* C*c*P gene (SO2178) recombinantly in *E. coli* as a maltose-binding protein fusion that has been previously described (21), as well as the presumed redox partner for *So* C*c*P, a monoheme cytochrome *c*5, SO0264 (21). We show, based on EPR, UV/Visible spectroscopy, and steady-state kinetics of recombinant *So* C*c*P, that the *So* C*c*P is a conventional *Psa*-type BC*c*P requiring reductive activation. We find that the as-isolated form of *So* C*c*P undergoes rapid reductive activation under *in vitro* assay conditions, with a rate that depends on the concentration of the electron donor. We present a

computational model for the peroxidase activity of as-isolated *So* C*c*P that permits the deconvolution of the reductive activation rate and the peroxide turnover rate from the enzymatic progress curves. Following our initial characterization of the *So* C*c*P system, we demonstrate that this protein serves as a facile model system for structure/function analysis through further investigation the role of the activation loops of *So* C*c*P. We show that mutations in loop 1 and loop 3 regions do not completely inhibit peroxidase activity, but instead show defects in peroxidase turnover and increases in the activation rate.

Materials and Methods

Expression and Purification of Diheme Cytochrome c Peroxidase from *Shewanella oneidensis*

The gene coding for the *Shewanella* cytochrome *c* peroxidase (SO2178) in the parent vector pMKL1 was a kind gift to our laboratory from Drs. Frank Collart and Yuri Londer (Argonne National Labs). The SO2178 gene is expressed as a fusion to the C-terminus of the maltose-binding protein (MBP), with a TEV site between the MBP and *So* C*c*P to allow isolation of a tag-free *So* C*c*P protein. The MBP protein also includes an N-terminal hexahistidine tag for Ni^{2+} affinity purification. The *So* C*c*P-MBP fusion protein is expressed in *E. coli* JM109 cells (Strategene). Maximal *So* C*c*P expression was achieved by co-transformation with pEC86, a plasmid bearing the cytochrome *c* maturation cassette (22). Transformed cells were grown in 10 mL starter culture at 37 °C for 8 hours. Starter cultures were resuspended into fresh media and used to inoculate bulk expression cultures containing 1 L of 2× YT (Fisher BioReagents) supplemented with 100 μg/ml ampicillin and 25 μg/ml chloramphenicol in a 2 L flask. Bulk expressions were grown at 37 °C for 14 to 16 hours with good aeration (200 rpm) to high optical density (A_{600} > 2). Induction for 4 hours with 80 mg/L of IPTG yielded pink to brown pellets as an indication of cytochrome *c* production. Cells were harvested, sonicated in 20mM Tris pH 7.4, 150 mM NaCl, 100 μM EDTA, 0.13 mg/mL lysozyme, clarified by centrifugation, and immediately loaded onto an amylose affinity resin column (NEB) to avoid proteolytic cleavage of the C*c*P-MBP fusion. For sensitive applications requiring very pure sample, amylose chromatography was followed by size exclusion chromatography on an S-100 column (GE Healthcare prepacked HiPrep™ Sephacryl™). Removal of MBP was achieved by cleavage overnight with TEV protease and subsequent Ni^{2+}-NTA chromatography. *So* CcP mutants in loop 1 (P75T/H81K/E84Q) and loop 3 (M219Q/F247N) were constructed using the QuikChange Mutagenesis Kit (Stratagene; see Supporting Information), and expressed and purified as MBP fusions as described for the wild-type protein.

Expression and Purification of Recombinant *Pseudomonas aeruginosa* Azurin

The plasmid pETAz9^{+} was a kind gift of Michelle McGuirl (UMontana). The plasmid was transformed into *E. coli* BL21(DE3), and the transformants were grown in 4 mL starter cultures of 2× YT until cloudy. Starter cultures were used to inoculate 1 L cultures of 2× YT with 50 μg/mL kanamycin for bulk expression. The 1L cultures were grown at 37 °C overnight to reach high optical density, and induced in the morning with 1 mM IPTG for 4 hours. The resulting cells were lysed gently by sonication in buffer containing 20 mM Tris pH 8, 20% glucose, 15 μg/mL lysozyme and 5 μg/mL DNase. Clarified lysate was supplemented with 100 μM final concentration of $CuSO_4$, and holo-azurin was loaded on Q-Sepharose equilibrated in 10 mM diethanolamine pH 9. Azurin was eluted with 500mM NaCl in 10 mM diethanolamine pH 9.00. Azurin-containg fractions were reduced with 1 mM dithionite and further purified by size exclusion chromatography (GE Healthcare prepacked HiPrep™ Sephacryl™S-100).

Expression and purification of *Shewanella oneidensis* cytochrome c5

The *Shewanella oneidensis* gene SO0264, which codes for cytochrome *c*5, was synthesized by Genewiz and sub-cloned into pET25b+ (Invitrogen) at the EcoRV restriction site. The resulting plasmid was named pSOc5, and was used for the expression of a tag-free version of the cytochrome bearing the wild-type periplasmic localization sequence at the N-terminus. Recombinant *S. oneidensis c*5 was expressed in *E. coli* BL21(DE3) carrying the pEC86 plasmid (22). For over-expression, 1 L of 2× YT media containing 100 μg/mL ampicillin and 25 μg/mL chloramphenicol was inoculated with 5 mL of resuspended overnight BL21(DE3)/pEC86/pSOc5 culture and grown without IPTG induction at 37 °C for 22 hours with moderate shaking (170 rpm). Cell pellets were harvested by centrifugation, resuspended in 80 mL of lysis buffer (20 mM Tris pH 8, 1 mM EDTA, 50 mM NaCl, 0.1 mg/mL lysozyme), and lysed by sonication. Lysate was clarified by centrifugation, the pH of the clarified lysate was adjusted to 4.5 by drop-wise addition of 1 M acetic acid, and precipitated proteins were removed by centrifugation. The resulting pink supernatant was oxidized by addition of equimolar potassium ferricyanide and loaded onto MacroPrep HighS resin (10 mL bed volume, BioRad) equilibrated in 10 mM sodium acetate pH 4.5. Bound proteins were eluted with an 80 mL gradient from 50 to 500 mM NaCl in 10 mM sodium acetate pH 4.5. *So* cyt *c***5** eluted in a broad peak centered around 250 mM NaCl, and fractions with purity ratios (A_{410}/A_{280}) of 4.0 or greater were pooled and stored in 15% glycerol at −80°C.

EPR Spectroscopy

X-band (9.62 GHz) EPR spectra were recorded on a Bruker 300 spectrometer equipped with an Oxford ESR-910 liquid helium cryostat. The quantification of all signals is relative to a Cu-EDTA spin standard. For quantification, the spectra were recorded under non-saturating microwave conditions, meaning that the signal intensity was found to be proportional to the square root of the microwave power. The EPR spectrum of the Cu-EDTA standard is recorded daily at a temperature and microwave power of 10K and 2μW. The copper concentration of the standard is determined by atomic absorption. The microwave frequency was calibrated with a frequency counter and the magnetic field with a NMR gaussmeter. The sample temperature was calibrated with a carbon-glass resistor (LakeShore CGR-1-1000) placed at the position of the sample in an NMR tube. A modulation frequency of 100 KHz with 10 G modulation amplitude was used for all EPR experiments. The EPR simulation software was written by one of the authors. The simulations are least-squares fits of the experimental spectra generated with consideration of all intensity factors, which allows computation of simulated spectra for a specified sample concentration. The simulations therefore allow a quantitative determination of protein signal intensities. The Windows software package (SpinCount) is available for general application to any mono- or dinuclear metal complex by contacting M. Hendrich.

Activity Assays

The electronic absorption spectra properties of the C*c*P-MBP and the tag-free C*c*P were conducted on a Cary 50 spectrophotometer (Varian). All assays were conducted at 23 °C in assay buffer (5 mM MES, 5 mM HEPES, 10 mM NaCl and 1 mM $CaCl_2$ at pH 6.00) following the protocol previously reported for the *P. denitrificans* enzyme (14). Horse heart cytochrome *c* (Sigma), *Psa* azurin, or *So* cyt *c***5** was reduced by treatment with 20 mM sodium L-sodium ascorbate, and excess ascorbate was removed from the electron donor by a PD-10 desalting column (NEB) immediately before the assay. A stock of between 5-10 μM enzyme was prepared in assay buffer. As-isolated proteins were treated with $K_3Fe(CN)_6$ to ensure that enzyme was the fully oxidized. Semi-reduced enzyme was prepared by incubation for at least 1 hour in 1 mM sodium L- ascorbate and 10 μM diaminodurol. The

oxidation of the reduced horse heart cytochrome *c* was monitored at 550 nm in the presence of H_2O_2 using an extinction coefficient difference between the oxidized and reduced protein of ($\Delta\varepsilon_{550}$) 21.5 $mM^{-1}cm^{-1}$ (23), whereas oxidation of reduced *So* cyt *c*5 was monitored at 553 nm using a difference in extinction coefficient of ($\Delta\varepsilon_{553}$) 12.5 ± 2 $mM^{-1}cm^{-1}$ as determined by comparison to protein concentrations determined by the BCA assay (Thermo Scientific). When azurin was used as the electron donor, the increase in absorbance at 628 nm is monitored using an extinction coefficient of ε_{628} = 5.0 $mM^{-1}cm^{-1}$ (24).

Lag-Phase Kinetics Model

A kinetic model for activation of the fully oxidized enzyme was implemented in Python 2.7, and the complete code is given in the Supporting Information. Because the concentration of active, semi-reduced C*c*P enzyme changes over the course of the experiment, the differential equations that describe the behavior of the system do not have a closed solution. Instead, we implement numerical integration with a time-step of 0.2 s to find an approximate analytical solution to the differential equations. Least-squares optimization was accomplished using the optimize.leastsq function in SciPy.

The amount of C*c*P converted from the as-isolated, oxidized state to the semi-reduced state during each time step depends on both the fraction of oxidized C*c*P that is bound to an electron donor and the rate of electron transfer in the bound complex. Based on the observation that even large concentrations of electron donor proteins (> 50 μM) are not saturating in the peroxidase assay, we assume that binding of oxidized C*c*P to the reduced electron donor (ED) protein has an equilibrium dissociation constant greater than 10 μM, and can be modeled by a rapid equilibrium. The fraction of oxidized C*c*P in the bound complex is given by:

$$f_B = \frac{[\mathrm{ED}]_{\mathrm{red}}}{[\mathrm{ED}]_{\mathrm{red}} + K_D}$$

where $[ED]_{red}$ is the concentration of reduced electron donor and K_D is the equilibrium dissociation constant for reduced electron donor binding to oxidized C*c*P.

During each time step, the concentration of semi-reduced C*c*P increases by the factor:

$$\Delta[\mathrm{CcP}]_{\mathrm{active}} = k_{\mathrm{act}} f_B [\mathrm{CcP}]_{\mathrm{inactive}}$$

where k_{act} is a rate constant with units of s^{-1} that describes the rate of electron transfer in the bound complex.

During each time step there are two ways for electron donor to become oxidized. The first is donating an electron to activate one molecule of C*c*P. The second is donating an electron to a molecule of C*c*P that has been oxidized by peroxide during the catalytic cycle. C*c*P must be recharged with two electrons during each catalytic cycle (6). The rate of peroxide catalysis depends on $[Cc P]_{active}$, and is first order in terms of the reduced electron donor concentration. To ensure the reaction is zero-th order in peroxide, we use peroxide concentrations in excess of 9 μM, an order of magnitude greater than the hydrogen peroxide K_m (see Results). The total change in the concentration of reduced electron donor at each time-step is:

$$\Delta[\mathrm{ED}]_{\mathrm{red}}=\Delta[\mathrm{CcP}]_{\mathrm{active}}+2k_1[\mathrm{CcP}]_{\mathrm{active}}[\mathrm{ED}]_{\mathrm{red}}$$

where k_1 is the second-order rate constant for the peroxide turnover. Mulitplying k_1 by the electron donor concentration gives as first-order rate constant that should match the k_{cat}^{obs} from Michaelis-Menten analysis.

Total absorbance is calculated using extinction coefficients for oxidized and reduced forms of the electron donor. For horse heart cytochrome *c*, ε(550 nm, oxidized) = 8.4 $mM^{-1}cm^{-1}$, ε(553 nm, reduced) = 29.9 $mM^{-1}cm^{-1}$ (23). For *Shewanella oneidensis* cyt *c*5, extinction coefficients were experimentally determined by comparison to BCA assay-derived concentrations, ε(553 nm, oxidized) = 5.1 ± 0.5 $mM^{-1}cm^{-1}$, ε(553 nm, reduced) = 17.6 ± 2 $mM^{-1}cm^{-1}$.

Following these three calculations, new values for $[CcP]_{active}$, $[CcP]_{inactive}$, $[ED]_{ox}$, and $[ED]_{red}$ are calculated, and used as initial values for the next time-step. For the best fit to the data, we include an additional time-dependent decay of the active *So* CcP into an inactive state.

Results

Expression and Purification of *So* CcP as an MBP Fusion

The bacterial diheme peroxidase from *Shewanella oneidensis* was overexpressed in *E. coli* JM109 as a soluble MBP fusion. Induction at high optical density (A_{600} > 1) and in the presence of the *c*-type cytochrome maturation cassette (*ccm*ABCDEFGH) (22) yields 10-25 mg of fusion protein per liter of culture. Because the presence of a fusion protein can change the activity of the protein of interest (25, 26), we proceeded to investigate whether the recombinant protein behaved like a native BC*c*P in biochemical assays.

Following removal of the MBP protein by TEV protease and Ni-NTA chromatography, the purity index (A_{408}/A_{280}) was typically around 4.8, matching previously reported values for a bacterial diheme peroxidases isolated from their native source (27). Because all bacterial diheme peroxidases have two hemes and a comparable number of tryptophan residues, a similar purity index suggests that a majority of the protein has the native heme loading. The MBP-fusion protein runs on an SDS-PAGE gel with an apparent molecular weight of 70 kDa, and the tag-free *So* C*c*P runs in a diffuse band with an apparent molecular weight of 35 kDa (Figure S1), consistent with the size predicted by the expressed amino acid sequence. Like all other reported BC*c*Ps, both the MBP-fusion and tag-free *So* C*c*P proteins run as a dimer in size-exclusion chromatography (Figure S2) (16, 19, 20, 28).

Optical Properties of the CcP-MBP Fusion and Tag-free CcP

The optical absorbance spectra of fully oxidized verses semi-reduced *So* C*c*P, both as an MBP-fusion protein and with the MBP tag removed, are shown in Figure 3. The spectral features at wavelengths greater than 300 nm characteristic of heme absorption are virtually identical in the MBP-fusion *So* C*c*P verses the tag-free *So* C*c*P, suggesting that the heme environments are not substantially affected by the presence of the fusion protein. The fusion protein has a higher absorbance at 280 nm, consistent with the presence of additional tryptophans in the MBP tag. Semi-reduced samples have extremely high absorbance at wavelengths below 300 nm due to the presence of excess sodium L-ascorbate, which is required to keep the sample in the semi-reduced state.

Fully oxidized *So* C*c*P shows a characteristic Soret maximum at 407 nm and broad β- and α-bands at 540 and 553 nm. The fully oxidized enzyme does not display the 640 nm band indicative of high-spin heme (Figure 3, inset). Upon reduction with L-ascorbate, the Soret band maximum shifts to 417 nm and a Soret shoulder around 407 nm persists, the β- and α-bands at 540 and 553 nm dramatically sharpen (consistent with the reduction of the H-heme (29)), and a charge transfer band at around 640 nm, suggestive of a high-spin ferric heme state, is clearly apparent (Figure 3, inset).

EPR Properties of the CcP-MBP and Tag-free CcP

The fully oxidized state of *So* C*c*P shows two low-spin ferric species (Figure 4A) in equal amounts. The signal at g = 3.40 is from a highly anisotropic low-spin species observed in all bacterial diheme peroxidases in their as-isolated state (both hemes in the ferric state) and originates from the H-Heme of the protein (17, 19, 30, 31). Species with $g = 3.0, 2.21, 1.30$ (L_1-Heme) originate from the L-Heme and have *g*-values similar to that of the *Psa*-type peroxidases (31, 32). The simulation overlaid on the data quantitatively agrees with the total heme concentration of the sample, and from the simulation, the two heme species are found to be present in equal amount. *So* C*c*P does not show a high-spin ferric signal near $g = 6$, which is a minority species in other diheme peroxidases (Figure S3) (17, 19, 29, 30, 33). Upon reduction with ascorbate the H-Heme signal disappears (Figure 4B), suggesting conversion of the ferric H-Heme to an EPR silent low-spin ferrous species as observed in other peroxidases. The signal from L_1-Heme loses intensity and a new low-spin heme species with $g = 2.87, 2.36, 1.51$ (L_2-Heme) appears. This change can be attributed to the conversion of a fraction of the low-potential species into the new L_2-Heme species. The concentrations of L_1- and L_2-Heme in the semi-reduced C*c*P together account for the concentration of low-potential heme before reduction. Table 1 summarizes the various species in the oxidized and semi-reduced enzyme with their amounts obtained from quantitative simulations.

Tag-free *So* C*c*P (Figure 4C) shows the same H-Heme species and L_1-Heme species as the fusion protein, but both at an overall lower amount (Table 1). In addition, a new feature is observed at $g = 2.97$. The new signal represents a significant amount of heme and overlaps with the $g = 3.10$ signal of the L_1-Heme. As shown by the simulation on Figure 4C, the spectrum can be accurately simulated with three heme species, using the same parameters as H- and L_1-Heme species, and a new heme site with $g = 2.97, 2.26, 1.52$ (TF-Heme). The simulations indicate that the concentrations of the H- and L_1-Heme species are approximately equal, and both lower in amount commensurate with the amount of the TF-Heme present. Thus, the new TF-Heme species appears at the expense of both H- and L_1-Heme species. For the semi-reduced tag-free protein (Figure 4D), the signal $g = 3.40$ vanishes indicating full reduction of the H-Heme. The signal (shoulder) at $g = 3.1$ decreases and the signal from the L_2-Heme is clearly visible at $g = 2.36$. The simulation shown in Figure 4D use the same parameters for L_1-, L_2- and TF-Hemes as that of Figure 4B or 4C, except in different amounts. The percentages of species determined from the simulation are given in Table 1. The relative amounts of the L_1-Heme and L_2-Heme are consistent with that observed from the fusion protein. The TF-Heme species in the semi-reduced sample is not affected by ascorbate addition and the amount of this species remains the same before and after reduction.

Catalytic Properties of So CcP

The activity of *So* C*c*P was determined in the presence of micromolar concentrations of various redox partners (Table 2). *So* cyt *c*5 is the presumed native electron donor in the periplasm of *Shewanella*, whereas horse heart cyt *c* and azurin are electron donors that have been previously used for kinetic analysis of BC*c*Ps, and are included in this study for

comparison. We determined kinetic parameters for both MBP-fusion *So* C*c*P and the tag-free *So* C*c*P. The linear initial rates (for semi-reduced protein) or fastest linear phases (for oxidized protein) at various concentrations of peroxide were used to calculate kinetic parameters using the Michaelis-Menten formalism (Table 2; Figure S4). Because the electron donor proteins bind extremely weakly to *So* C*c*P (K_m > 10 μM), we could not achieve saturating concentrations *in vitro* using any of the electron donors studied, and as a result the values reported below are not maximal turnover rates.

Qualitative inspection of the progress curves reveals that while the oxidation of electron donor occurs in a typical manner for reactions initiated by semi-reduced enzyme (Figure 5A), a distinct lag phase is observed when fully oxidized *So* C*c*P is used (Figure 5B). The lag phase reflects the conversion of the oxidized state to the active, semi-reduced state *in vitro*. In all cases, k_{cat}^{obs} values for the semi-reduced *So* C*c*P are faster than the oxidized *So* C*c*P. We suspect that this is partially because of a time-dependent deactivation of the C*c*P during the several minute time course of the experiment. We have seen that for both semi-reduced and oxidized *So* C*c*P, the electron donor is not completely oxidized at the endpoint of the experiment if the initial rate is not sufficiently fast (data not shown).

Kinetic parameters for *So* C*c*P vary depending on the electron donor used or the presence of the MBP tag. For the non-native electron donors horse heart cyt *c* and azurin, peroxide turnover of the MBP-tagged *So* C*c*P is approximately 10 times faster than for the native, tag-free form in the same oxidation state. In contrast, when *So* cyt *c*5 is used the opposite is true; peroxide turnover rates for the tag-free protein are 7 to 10 times faster for the tag-free form of the protein than for the MBP-tagged protein, suggesting that the MBP tag affects the rate-limiting step of turnover.

Peroxide binding as assessed by K_m values is the same, within error, for almost all combinations of peroxidase and electron donor assayed. A notable exception is that K_m values are generally two times weaker for the oxidized form of the enzyme when compared to the semi-reduced form under the same conditions, which may reflect an incomplete activation of the oxidized protein on the time-scale of the *in vitro* assay.

Comparison of Peroxide Turnover to Other BCcP Family Members

Peroxide turnover kinetics have been reported for numerous members of the BC*c*P family (Table 3). Among the BC*c*Ps in Table 3, all have estimated or measured K_m values for electron donors greater than 50 μM (17, 20, 24, 34). Because peroxide turnover was measured at concentrations much less than the K_m, the rate of the reaction is approximately linearly proportional to the electron donor concentration. In this linear range, the peroxide turnover divided by the electron donor concentration ($k_{cat}^{obs}/[ED]$) gives an effective bimolecular rate constant that can be compared between the BC*c*Ps. The value of $k_{cat}^{obs}/[ED]$ for *So* C*c*P is the fastest of all of the BC*c*Ps we surveyed. *So* C*c*P also has the tightest peroxide binding, as measured by K_m.

Computational Modeling of Lag-Phase Kinetics

Our simple kinetics model, which considers an equilibrium binding step, an activation step, and a peroxidase turnover step, recapitulates the shape of the peroxide turnover progress curve (Figure 5C). Residuals are very small but nonrandom, suggesting a minor systematic error of unknown origin.

Implementing the computational model requires us to make some educated hypotheses about the *So* C*c*P:*So* cyt *c*5 system. The model contains two different parameters, the activation rate and the dissociation constant for binding of the electron donor to *So* C*c*P, either of which could effect the length of the lag phase. Neither of these parameters has been

measured independently for *So* C*c*P and *So* cyt *c*5. In our model, we are unable to separate the effect of the activation rate constant from that of the equilibrium dissociation constant of the oxidized form of *So* C*c*P for the reduced electron donor. We therefore implement the model by keeping the equilibrium dissociation constant the same (7μM) for all cases. This value for K_D is in the range of equilibrium binding constants previously reported for BC*c*Ps and monoheme electron donor proteins (9). Differences in the activation rates that we report (k_{act}) reflect either changes in electron transfer rate or differences in binding of the electron donor.

Analysis of lag-phase kinetics using the computational model (Table 4) confirms the results from Michealis-Menten analysis. The MBP-fusion *So* C*c*P turns over peroxide at approximately the same rate with either horse heart cyt *c* or *So* cyt *c*5 as the electron donor, whereas the tag-free *So* C*c*P turns over peroxide 25 times more rapidly with the native electron donor *So* cyt *c*5 when compared to horse heart cyt *c*. Activation rates are significantly slowed when tag-free *So* C*c*P is assayed in the presence of horse heart cyt *c* as the electron donor. This suggests that horse heart cyt *c* binds to the tag-free protein either more weakly or in a conformation that gives less efficient electron transfer.

Characterization of Activation Loop Mutants

Additional kinetic analyses were performed for two tag-free *So* C*c*P variants containing mutations in two of the three loops that are known to undergo conformational changes upon reductive activation of a *Psa*-type C*c*P (depicted in Figure 1): either loop 1 (P75T/H81K/E84Q) or loop 3 (M219Q/F247N). We did not make mutations in the loop 2 region because the amino acid sequence of the *So* enzyme already matches that of the *Ne* C*c*P in all key positions that are different between the two functional sub-classes. The visible absorbance spectra of both *So* C*c*P variants in the semi-reduced and oxidized states are identical when compared to spectrum of the wild-type protein in the same oxidation state (data not shown), indicating that the protein variants are folded with hemes in a similar environment as the wild-type enzyme. Despite the location of the mutations (many of which are far from the presumed peroxide binding site), both variants show defects in peroxide turnover (Table 5), suggesting that the wild-type enzyme is highly optimized for a high rate of peroxide turnover. The triple mutant in loop 1, P75T/H81K/E84Q, shows a five-fold decrease in turnover of the semi-reduced state and 20-fold decrease in turnover of the oxidized state when compared to the wild-type protein under identical conditions. The double mutant M219Q/F247N shows a slightly larger defect in peroxide turnover in the semi-reduced state, a 12-fold decrease when compared to wild-type protein under identical conditions. Peroxide binding for the semi-reduced state of the mutants, as measured by K_m, is unchanged (within error) for the mutants when compared to wild-type, but both mutants show a slight increase of the K_m of the oxidized state for peroxide. The *So* C*c*P protein variants also demonstrated lag-phase kinetics for peroxide turnover when initiated by oxidized enzyme. For the loop 1 triple mutant, the activation rate is 7 times faster than wild-type, and the loop 3 double mutant shows a very slight increase in activation rate over the wild-type protein.

The kinetic differences noted for these two constructs were reflected in differences in their EPR characterization: whereas the fully-oxidized wild-type MBP-tagged enzyme reveals two states H (g = 3.37, 2.20, 1.50) and L_1 (g= 3.08, 2.26, 1.30) corresponding to the H- and L-hemes, both the loop 1 triple mutant and the loop 3 double mutant additionally reveal significant population of states L_2 and TF (Figure S5). Thus, substantial amounts (Table S1) of oxidized MBP-enzymes have already adopted conformations that would be associated activated L-heme (*i.e.,* the L_2 state). Consequently, the presence of lag-phase kinetics is at present unclear. The lower activities of the variants do not quantitately correlated with the presence of the TF-heme. If we assume that the TF-heme state is inactive, we would expect at most a factor of two decrease in activity, yet activity is decreased by approximately an

order of magnitude. We suspect, but cannot yet substantiate, that the conformational changes observed in the EPR spectra of the oxidized states of the variants reflect changes in access to the hemes, their redox properties, or the ability of specific enzymatic states to inter-convert, as required for catalysis.

Discussion

Optical Spectroscopy of So CcP

The electronic absorption spectra of the as-isolated state of the MBP-fusion and tag-free *So* C*c*P both exhibit the Soret maximum at 407 nm characteristic of ferric *c*-type hemes. Changes to the spectrum upon reduction with ascorbate or dithionite mirror changes that have been seen other BC*c*Ps (15, 16, 18, 19, 29): Reduction of the H-heme with ascorbate causes a red-shift in the Soret maximum to 417 nm and a sharpening of the β- and α-bands at 540 nm and 553 nm, while the ascorbate-reduced spectrum maintains a Soret feature at 407 nm, indicating that one heme remains in the ferric state. Further reduction with dithionite results in the disappearance of the Soret shoulder and an increase in the intensity of the Soret peak at 417 nm (data not shown). Intriguingly, the only significant differences in the optical characteristics of the *So* enzyme, with respect to canonical C*c*Ps is the absence of a 640 nm band with the fully oxidized enzyme. As observed in the *Pd* and *Psa* enzymes, the 640 nm band has been attributed to a high-spin state of the high-potential heme (29,30,33)). Thus, the *So* enzyme appears to possess a low-spin H-heme. However, the 640 nm band is observed in the semi-reduced protein, indicating the same high-spin state of the oxidized L-heme, in parallel with other BC*c*P enzymes that require reductive activation to attain activity (29,30,33)).

EPR Characterization of the So CcP

Comparisons of the *So* enzyme with other bacterial diheme peroxidases by electron paramagnetic resonance spectroscopy (EPR) demonstrates the similarity of *So* peroxidase to the *Psa* (30) and *Pd* (31) peroxidases in both its oxidized and semi-reduced form, as compared to the *Ne* and *Mc* peroxidases. In the oxidized state, the g_z-value (3.10) of the L-Heme is closer to that of *Pd* (3.00) than *Ne* (2.85). In the semi-reduced state of both the *So* and *Pd* enzymes, a fraction of the L-heme changes to a new species, whereas no such change occurs for the *Ne* enzyme. Contrasting the optical spectroscopy, we observe no evidence in the EPR for conversion of heme to the high-spin state as has been previously observed for the *Psa* enzyme (30). For the *So* enzyme, the two L-Heme species represent 34% and 20% of the heme in the sample after ascorbate addition. Based on the *g*-values, the new L_2-heme species falls into the imidazolate classification of EPR signals: using the crystal-field parameters of Taylor (35), $\Delta/\lambda = 2.736$ and $v/\Delta = 0.762$ for L_2, while L_1 displays analogous parameters that are indicative of neutral imidazole binding ($\Delta/\lambda = 2.687$ and $v/\Delta = 0.524$). Thus, it appears that upon semi-reduction the axial His for 40% of the L-heme is deprotonated. For all these enzymes, the g_z-values of the H-heme are approximately the same, and this heme is reduced with ascorbate in the semi-reduced form. Approximately one-half of the tag-free *So* C*c*P protein appears to be the same as the fusion protein. The signals are in the same locations, and upon ascorbate addition, this fraction of the protein undergoes the same spectroscopic changes as that observed for the fusion protein: H-heme vanishes and a fraction of the L-Heme changes to a second species. The spectrum of the tag-free protein, however, has a significant additional new low-spin heme species (TF-heme) with $g_z = 2.97$ relative to the MBP-fusion protein. This TF-heme also appears to be a *bis*-His heme based on the *g*-values (with crystal-field parameters that make distinguishing between neutral His and imidazolate character ambiguous). The amount of TF-heme is approximately equal to that of the normal heme species, which suggest that approximately one-half of the

protein is in this other state. The addition of ascorbate to the tag-free protein had no effect on the state ascribed to the TF-heme, suggesting that it cannot be reduced by ascorbate.

The molecular basis of the generation of the new TF-heme state is unclear at this time, and because the visible absorbance spectra of tag-free enzyme are nearly identical to the MBP-fusion, it is presumed that the generation of the TF-heme state may be reversible at room temperature. However, these data do imply that there are inherent differences in conformational flexibility in the MBP-tagged verses the tag-free forms of the *So* C*c*P enzyme, consistent with the differences seen in the kinetics of peroxide turnover and activation rate in the two forms of the enzyme.

Catalytic behavior of *So* CcP

We monitored the kinetic parameters of peroxide turnover and activation of *So* C*c*P in the presence of several electron donor proteins as well as for MBP-tagged and tag-free versions of the enzyme. It is clear that the kinetic behavior of the MBP-tagged protein differs substantially from the tag-free protein; without the MBP-tag, *So* cyt *c*5 gives the highest peroxide turnover, whereas the MBP-tagged protein is most active when horse heart cyt *c* or azurin are used as electron donors. These data indicate that the relatively large MBP protein has a principle effect on the binding of electron donors.

It is surprising that the peroxide turnover rates of the oxidized protein never reach the rates of the semi-reduced proteins. This may indicate that there is a slow step in reductive activation that is required for maximum turnover efficiency and is not attained during the time course of the *in vitro* experiments. This is supported by the observation that peroxide binding (K_m) differs between oxidized and semi-reduced *So* C*c*P. The slow time-dependent decay of activated protein, which was required for optimal fit of the computation model to the lag-phase data, may also contribute to the rate differences. One possible explanation for this deactivation is dissociation of the dimeric *So* C*c*P at the low nanomolar concentrations in the *in vitro* assay (14).

The catalytic parameters we report for peroxide turnover of *So* C*c*P in the presence of various electron donors are in the same range as those reported for other BC*c*Ps elsewhere in the literature. *So* C*c*P binds peroxide much more tightly, as assayed by K_m values, than other representative BC*c*Ps. This may reflect a difference in peroxide sensitivity of components of the *Shewanella* periplasm when compared with other gram negative bacteria. The values of k_{cat}^{obs} reported in Table 3 are not the maximum values for the BC*c*P enzymes; maximum peroxide turnover, in the presence of saturating electron donor, will be several times higher. Given the reported concentrations of *So* c5 isolated from cells grown under low oxygen conditions (34 micromoles of c5 per kilogram of cell pellet; 36), we estimate that the *in vivo* concentration of *So* cyt *c*5 in the periplasm is on the order of 300 μM, suggesting that *in vivo* rates of peroxide turnover will be much faster than those reported here, where the maximum cyt *c*5 concentration used is 40 μM (with the relationship between peroxide turnover and electron donor concentration being linear).

Studies with other BC*c*Ps have demonstrated that a variety of small proteins can act as electron donors, and that the peroxide turnover rate of the BC*c*P depends on the identity of the electron donor (37). This variability is attributed to differences the binding orientation of the various electron donors. In the case of *Pd* C*c*P, computational modeling and NMR identified two possible electron donor binding sites: one that was favored by horse heart cytochrome *c* and a different binding site favored by the native *Pd* electron donor cytochrome *c*-550 (8, 9). Our data suggest a similar model for *So* C*c*P. For *So* C*c*P, peroxide turnover is most efficient for the tag-free protein when the native electron donor *So* cyt *c*5 is used, suggesting that *So* cyt *c*5 binds to the *So* C*c*P surface in a unique mode that is

optimized for electron transfer. The lower turnover rates for non-native electron donors may result from binding more weakly to the *So* C*c*P surface, or in a slightly different orientation that is less optimal for electron transfer. Moreover, we show that the presence of the MBP-tag favors the turnover of peroxide in the presence of the non-native electron donors azurin and horse heart cyt *c*. This suggests that the bulky MBP protein either increases the binding affinity of non-native electron donors, or forces the non-native electron donor to bind in a mode that facilitates more rapid electron transfer.

Previous studies of BC*c*P family members and electron donor proteins have suggested that the electrostatic potential of the protein surfaces allows the native electron donor to select a proper binding site. *So* cyt *c*5 has an equal number of positive and negative amino acids, but the arrangement of positive and negative charges results in a substantial dipole moment (0.56 D/atom) (38). Horse heart cytochrome *c* has an excess of positively charged residues, but the arrangement of charges results in a lower net dipole (0.324 D/atom). This difference in the electrostatic potential of the two electron donors may contribute to the differences in binding mode. We are currently undertaking biophysical experiments to explore the differences in the equilibrium binding between electron donors and various forms of the *So* C*c*P protein.

Tag-free vs. MBP-fusion So CcP

The *So* C*c*P protein was expressed in *E. coli* with an N-terminal MBP fusion. This fusion protein system allows purification of the *So* C*c*P protein in high yield, an important criterion for use as a model BC*c*P in biophysical studies. We therefore investigated the potential differences between the *So* C*c*P-MBP fusion protein and the tag-free *So* C*c*P. Optical spectroscopy failed to show any differences between the heme environment in the fusion protein verses the tag-free protein. However, EPR spectroscopy demonstrates that the tag-free protein has greater conformational flexibility than *So* C*c*P-MBP, as half of the tag-free *So* CcP was trapped in a “TF-heme” state in the low-temperature EPR experiments. The peroxidase turnover data suggests that this additional conformational flexibility facilitates interaction with the native electron donor *So* cyt *c*5, resulting in higher rates of peroxide turnover. We conclude that the MBP fusion protein affects the conformational flexibility, but not the underlying fold, of the *So* C*c*P protein, demonstrating that fusion proteins should be employed carefully in biochemical and biophysical studies.

Kinetics Modeling and Comparison to Other BCcPs

Previous reports (39) have investigated the lag-phase behavior of the model BC*c*P family member from *Pseudomonas aeruginosa*. The authors noted, as we do in this report, that the lag-phase behavior may result from equilibrium binding between oxidized C*c*P and reduced electron donor followed by electron transfer, which can be modeled using an equilibrium binding constant and an activation rate. The authors reported kinetic parameters (K_m = 4 μM and k_{act} = 0.2 s^{-1}) (39) that agree remarkably well with those we have established for *So* C*c*P. Our use of a modern computational framework in Python and SciPy allows us to quickly extract the activation and peroxidase rates from the kinetic progress curve. The framework we developed has been used here and in continuing experiments to study the differential effects of mutations on the activation or the peroxide turnover rate.

Effect of Activation Loop Mutations on Activation and Peroxide Turnover

There are few reports of mutagenesis studies of BC*c*P family members. With the exception of the *Geobacter* C*c*P loop 2 mutation (18), reports have been limited to mutation of residues with hypothesized roles in heme ligation, proton-delivery or electron transfer between the hemes (40, 41). In general, these mutational studies have resulted in complete deactivation of the peroxide turnover activity of the enzyme, and full kinetic characterization has been

rarely reported (40, 41). In this study, we focus on mutations in flexible regions that are not spcificially implicated in catalysis. These locations can be mapped on to the fully oxidized *Psa* C*c*P x-ray crystal structure, as shown in Figure 6, which demonstrates that in the case of the M219Q/F247N double mutation, both positions are well removed from the low-potential catalytic heme.

A sequence alignment of *Ne* and *So* C*c*Ps shows extremely strong sequence conservation in several loop regions. Based on this sequence conservation and the structural evidence of the importance of these loops in the conformational change required for activation, we predicted that the *So* C*c*P would not require reductive activation. However, UV/Visible spectroscopy, EPR spectroscopy, and peroxide turnover indicate that this is not the case. We therefore sought to make mutations in the activation loops of *So* C*c*P in an attempt to convert *So* CcP into a *Ne*-type BC*c*P. For the BC*c*P of *Geobacter sulfurreducens*, the S134P/V135K double mutant transforms the L-loop (loop 1) into an “always open” state, as determined crystallographically (18). In attempting a similar conversion, we constructed *So* C*c*P mutations in loop 1 (P75T/H81K/E84Q) and loop 3 (M219Q/F247N). We did not make mutations in the loop 2 region because the sequences are already nearly identical between *So* and *Ne* C*c*Ps; the only differences are in positions otherwise conserved between *Psa*- and *Ne*-type BCcPs that are not likely to be important in reductive activation.

We found that neither set of mutations successfully transformed *So* C*c*P into a constitutive, *Ne*-type BC*c*P. However, the loop 1 triple mutation (P75T/H81K/E84Q) was activated much more quickly than the wild-type protein during the *in vitro* peroxidase turnover assay. This suggests that the three simultaneous mutations have successfully modulated the structure of loop 1 to favor the active state. Mutations in the loop regions were accompanied by severe decreases in peroxidase activity for the *So* C*c*P variants, indicating that the mutations have additional effects on catalytic activity in addition to changes on the equilibrium between the active and inactive states. Interestingly, the M219Q/F247N mutation affects catalysis despite its location near the H-heme, far from the catalytic site. This suggests that the M219Q/F247N mutation also has a subtle impact on the equilibrium between the inactive and active conformations of the protein. Indeed, the EPR characterization of either of the two mutants described here underscore that structural conformations around the H-heme are strongly affected by the sequences of loops 1 and 3. The loop 1 and loop 3 mutants both reveal that multiple heme states can be adopted, while fully oxidized, which presumably negatively impact catalytic competency. And, while the tag-free version of the loop 3 M219Q/F247N mutant appears similar to native enzyme, the L-heme clearly displays slight perturbations in *g* values, suggesting that the electronic structure of the L-heme is not truly native-like. Together, these data strongly suggest that all of the flexible loop regions identified in other BC*c*P family members are also important for redox-coupled conformational changes in the *So* C*c*P.

Conclusions

This study describes the recombinant expression and characterization of a BC*c*P family member, the *So* C*c*P. UV/Visible spectroscopy and EPR spectroscopy confirm the similarity between *So* C*c*P and other *Psa*-like peroxidases, while EPR also suggests subtle differences in the conformational flexibility of the *So* C*c*P when compared to other bacterial peroxidases. Peroxide turnover of *So* C*c*P can be monitored using a variety of native and non-native electron donor proteins, and Michaelis-Menten analysis confirms that *So* C*c*P catalyzes the turnover of peroxide with catalytic efficiencies similar to other documented BC*c*Ps. The *So* C*c*P can be easily purified in high yield from the *E. coli* system, and sequence variants have proven easy to express and purify, making *So* C*c*P an excellent system for mutational study. We hope that the detailed kinetic characterization we present

here can serve to initiate extensive mechanistic study of the BC*c*P family, and more broadly, the mechanism of electron transfer in proteins.

Supplementary Material

Refer to Web version on PubMed Central for supplementary material.

Acknowledgments

The authors wish to thank Drs. Frank Collart and Yuri Londer (Argonne), Michelle McGuirl (UMontana) and Mr. Ben Levin for their kind supply of reagents used in this work.

References

1. Chandel NS, McClintock DS, Feliciano CE, Wood TM, Melendez JA, Rodriguez AM, Schumacker PT. Reactive oxygen species generated at mitochondrial complex III stabilize hypoxia-inducible factor-1alpha during hypoxia: a mechanism of O2 sensing. J Biol Chem. 2000; 275:25130–25138. [PubMed: 10833514]
2. Halliwell B, Gutteridge JMC. Biologically relevant metal ion-dependent hydroxyl radical generation. FEBS Lett. 1992; 307:108–112. An update. [PubMed: 1322323]
3. Van Spanning RJ, De Boer AP, Reijnders WN, Westerhoff HV, Stouthamer AH, Van Der Oost J. FnrP and NNR of Paracoccus denitrificans are both members of the FNR family of transcriptional activators but have distinct roles in respiratory adaptation in response to oxygen limitation. Mol Microbiol. 1997; 23:893–907. [PubMed: 9076727]
4. Hiner A, Raven EL, Thorneley R, Garcia-Canovas F, Rodriguez-Lopez JN. Mechanisms of compound I formation in heme peroxidases. J Inorg Biochem. 2002; 91:27–34. [PubMed: 12121759]
5. Finzel BC, Poulos TL, Kraut J. Crystal structure of yeast cytochrome c peroxidase refined at 1.7-A resolution. J Biol Chem. 1984; 259:13027–13036. [PubMed: 6092361]
6. Ellfolk N, Ronnberg M, Aasa R, Andreasson LE, Vanngard T. Properties and function of the two hemes in Pseudomonas cytochrome c peroxidase. Biochim Biophys Acta. 1983; 743:23–30. [PubMed: 6297595]
7. Pettigrew GW, Echalier A, Pauleta SR. Structure and mechanism in the bacterial dihaem cytochrome c peroxidases. J Inorg Biochem. 2006; 100:551–67. [PubMed: 16434100]
8. Pettigrew GW, Prazeres S, Costa C, Palma N, Krippahl L, Moura I, Moura JJ. The structure of an electron transfer complex containing a cytochrome c and a peroxidase. J Biol Chem. 1999; 274:11383–9. [PubMed: 10196231]
9. Pettigrew GW, Pauleta SR, Goodhew CF, Cooper A, Nutley M, Jumel K, Harding SE, Costa C, Krippahl L, Moura I, Moura J. Electron transfer complexes of cytochrome c peroxidase from Paracoccus denitrificans containing more than one cytochrome. Biochemistry. 2003; 42:11968–11981. [PubMed: 14556628]
10. Ronnberg M, Ellfolk N. Pseudomonas cytochrome c peroxidase. Initial delay of the peroxidatic reaction Electron transfer properties. Biochim Biophys Acta. 1978; 504:60–66. [PubMed: 213111]
11. Echalier A, Goodhew CF, Pettigrew GW, Fulop V. Activation and catalysis of the di-heme cytochrome c peroxidase from Paracoccus pantotrophus. Structure. 2006; 14:107–117. [PubMed: 16407070]
12. Echalier A, Brittain T, Wright J, Boycheva S, Mortuza GB, Fulop V, Watmough NJ. Redox-linked structural changes associated with the formation of a catalytically competent form of the diheme cytochrome c peroxidase from Pseudomonas aeruginosa. Biochemistry. 2008; 47:1947–1956. [PubMed: 18217775]
13. Shimizu H, Schuller DJ, Lanzilotta WN, Sundaramoorthy M, Arciero DM, Hooper AB, Poulos TL. Crystal structure of Nitrosomonas europaea cytochrome c peroxidase and the structural basis for ligand switching in bacterial di-heme peroxidases. Biochemistry. 2001; 40:13483–13490. [PubMed: 11695895]

14. Gilmour R, Goodhew CF, Pettigrew GW, Prazeres S, Moura JJG, Moura I. The kinetics of the oxidation of cytochrome c by Paracoccus cytochrome c peroxidase. Biochem J. 1994; 300:907–914. [PubMed: 8010977]
15. Alves T, Besson S, Duarte LC, Pettigrew GW, Girio F, Devreese B, Vandenberghe I, Van Beeumen JJ, Fauque G, Moura I. A cytochrome c peroxidase from Pseudomonas nautica 617 active at high ionic strength: expression, purification and characterization. Biochim Biophys Acta Protein Struct Mol Enzymol. 1999; 1434:248–259.
16. De Smet L, Pettigrew GW, Van Beeumen JJ. Cloning, overproduction and characterization of cytochrome c peroxidase from the purple phototrophic bacterium Rhodobacter capsulatus. Eur J Biochem. 2001; 268:6559–6568. [PubMed: 11737210]
17. Timoteo CG, Tavares P, Goodhew CF, Duarte LC, Jumel K, Girio FMF, Harding S, Pettigrew GW, Moura I. Ca2+ and the bacterial peroxidases: the cytochrome c peroxidase from Pseudomonas stutzeri. J Biol Inorg Chem. 2003; 8:29–37. [PubMed: 12459896]
18. Hoffmann M, Seidel J, Einsle O. CcpA from Geobacter sulfurreducens is a basic di-heme cytochrome c peroxidase. J Mol Biol. 2009; 393:951–965. [PubMed: 19735665]
19. Arciero D, Hooper AB. A di-heme cytochrome c peroxidase from Nitrosomonas europaea catalytically active in both the oxidized and half-reduced states. J Biol Chem. 1994; 269:11878–11886. [PubMed: 8163487]
20. Zahn JA, Arciero DM, Hooper AB, Coats JR, DiSpirito AA. Cytochrome c peroxidase from Methylococcus capsulatus Bath. Arch Microbiol. 1997; 168:362–372. [PubMed: 9325424]
21. Londer YY, Giuliani SE, Peppler T, Collart FR. Addressing Shewanella oneidensis “cytochromome”: the first step towards high-throughput expression of cytochromes c. Protein Expression Purif. 2008; 62:128–137.
22. Arslan E, Schulz H, Zufferey R, Kunzler P, Thony-Meyer L. Overproduction of the Bradyrhizobium japonicum c-type cytochrome subunits of the cbb3 oxidase in Escherichia coli. Biochem Biophys Res Commun. 1998; 251:744–747. [PubMed: 9790980]
23. Van Gelder B, Slater EC. The extinction coefficient of cytochrome c. Biochim Biophys Acta. 1962; 58:593–5. [PubMed: 13897582]
24. Soininen R, Ellfolk N. Pseudomonas cytochrome c peroxidase. IV. Some kinetic properties of the peroxidations reaction, and enzymatic determination of the extinction coefficients of Pseudomonas cytochrome c-551 and azurin. Acta Chem Scand. 1972; 26:861–872. [PubMed: 4342882]
25. Mason AB, He QY, Halbrooks PJ, Everse SJ, Gumerov DR, Kaltashov IA, Smith VC, Hewitt J, MacGillivray RTA. Differential effect of a his tag at the N- and C-termini: functional studies with recombinant human serum transferrin. Biochemistry. 2002; 41:9448–9454. [PubMed: 12135367]
26. Song J, Markley JL. Cautionary tail: the presence of an N-terminal tag on dynein light-chain Roadblock/LC7 affects its interaction with a functional partner. Protein Pept Lett. 2007; 14:265–268. [PubMed: 17346231]
27. Goodhew CF, Wilson IB, Hunter DJ, Pettigrew GW. The cellular location and specificity of bacterial cytochrome c peroxidases. Biochem J. 1990; 271:707–712. [PubMed: 2173903]
28. Gilmour R, Prazeres S, McGinnity DF, Goodhew CF, Moura JJ, Moura I, Pettigrew GW. The affinity and specificity of Ca(2+)-binding sites of cytochrome-c peroxidase from Paracoccus denitrificans. Eur J Biochem. 1995; 234:878–86. [PubMed: 8575448]
29. Gilmour R, Goodhew CF, Pettigrew GW, Prazeres S, Moura I, Moura JJ. Spectroscopic characterization of cytochrome c peroxidase from Paracoccus denitrificans. Biochem J. 1993; 294:745–752. [PubMed: 8397509]
30. Foote N, Peterson J, Gadsby P, Greenwood C, Thomson A. Redox-linked spin-state changes in the di-haem cytochrome c-551 peroxidase from Pseudomonas aeruginosa. Biochem J. 1985; 230:227–237. [PubMed: 2996492]
31. Prazeres S, Moura JJ, Moura I, Gilmour R, Goodhew CF, Pettigrew GW, Ravi N, Huynh BH. Mossbauer characterization of Paracoccus denitrificans cytochrome c peroxidase. Further evidence for redox and calcium binding-induced heme-heme interaction. J Biol Chem. 1995; 270:24264–24269. [PubMed: 7592634]

32. Aasa R, Ellfolk N, Ronnberg M, Vanngard T. Electron paramagnetic resonance studies of Pseudomonas cytochrome c peroxidase. Biochim Biophys Acta. 1981; 670:170–175. [PubMed: 6271239]
33. Foote N, Peterson J, Gadsby PM, Greenwood C, Thomson AJ. A study of the oxidized form of Pseudomonas aeruginosa cytochrome c-551 peroxidase with the use of magnetic circular dichroism. Biochem J. 1984; 223:369–378. [PubMed: 6093773]
34. Hu W, De Smet L, Van Driessche G, Bartsch RG, Meyer TE, Cusanovich MA, Van Beeumen J. Characterization of cytochrome c-556 from the purple phototrophic bacterium Rhodobacter capsulatus as a cytochrome-c peroxidase. Eur J Biochem. 1998; 258:29–36. [PubMed: 9851688]
35. Taylor C. The EPR of low spin heme complexes: Relation of the tau2g hole model to the directional propertis of the g tensor, and a new method for calculating the ligand field parameters. Biochim Biophys Acta Protein Struct. 1977; 491:137–148.
36. Meyer TE, Tsapin AI, Vandenberghe I, DeSmet L, Frishman D, Nealson KH, Cusanovich MA, vanBeeumen JJ. Identification of 42 possible cytochrome c genes in the Shewanella oneidensis genome and characterization of six soluble cytochromes. OMICS. 2004; 8:57–77. [PubMed: 15107237]
37. Pauleta SR, Cooper A, Nutley M, Errington N, Harding S, Guerlesquin F, Goodhew CF, Moura I, Moura JJG, Pettigrew GW. A copper protein and a cytochrome bind at the same site on bacterial cytochrome c peroxidase. Biochemistry. 2004; 43:14566–14576. [PubMed: 15544327]
38. Felder CE, Prilusky J, Silman I, Sussman JL. A server and database for dipole moments of proteins. Nucleic Acids Res. 2007; 35:W512–521. [PubMed: 17526523]
39. Foote N, Turner R, Brittain T, Greenwood C. A quantitative model for the mechanism of action of the cytochrome c peroxidase of Pseudomonas aeruginosa. Biochem J. 1992; 283:839–843. [PubMed: 1317165]
40. De Smet L, Savvides SN, Van Horen E, Pettigrew G, Van Beeumen JJ. Structural and mutagenesis studies on the cytochrome c peroxidase from Rhodobacter capsulatus provide new insights into structure-function relationships of bacterial di-heme peroxidases. J Biol Chem. 2006; 281:4371–4379. [PubMed: 16314410]
41. Hsiao HC, Boycheva S, Watmough NJ, Brittain T. Activation of the cytochrome c peroxidase of Pseudomonas aeruginosa. The role of a heme-linked protein loop: a mutagenesis study. J Biol Inorg Chem. 2007; 101:1133–1139.

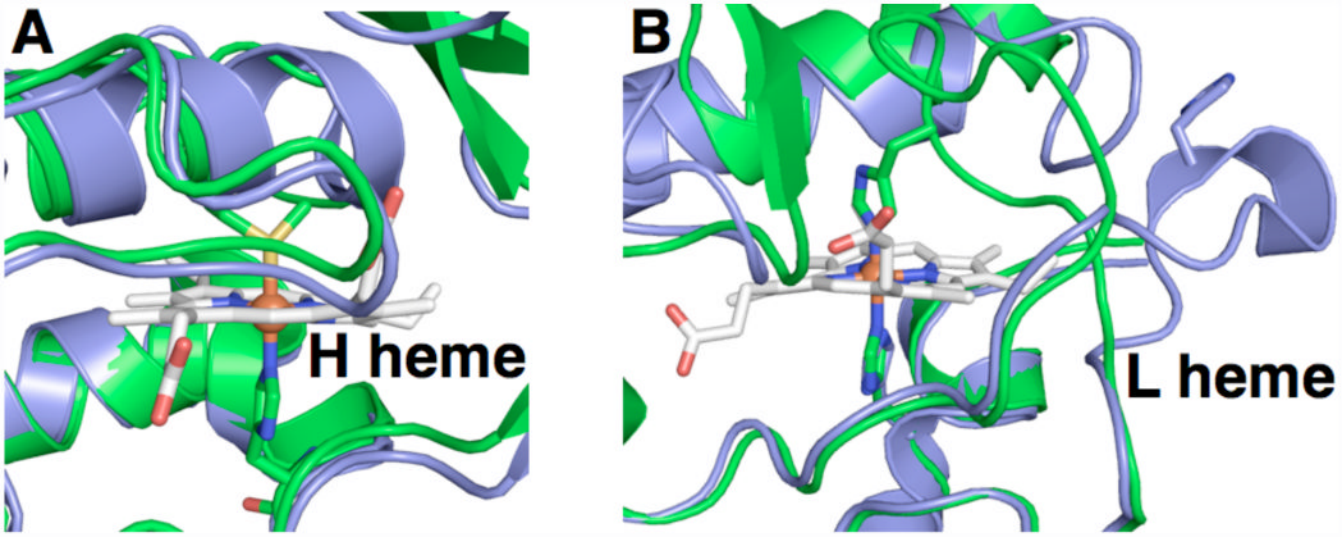

Figure 1.

Comparison of the structures of the inactivated (green) versus activated (blue) states of BC*c*Ps, focusing on the residues surrounding the high potential heme (A) and low potential heme (B). *Pseudomonas aeruginosa* cytochrome *c* peroxidase as-isolated is shown in green (PDB code = 1EB7); constitutively active cytochrome *c* peroxidase from *Nitrosomonas europaea* is shown in blue (PDB code = 1IQC).

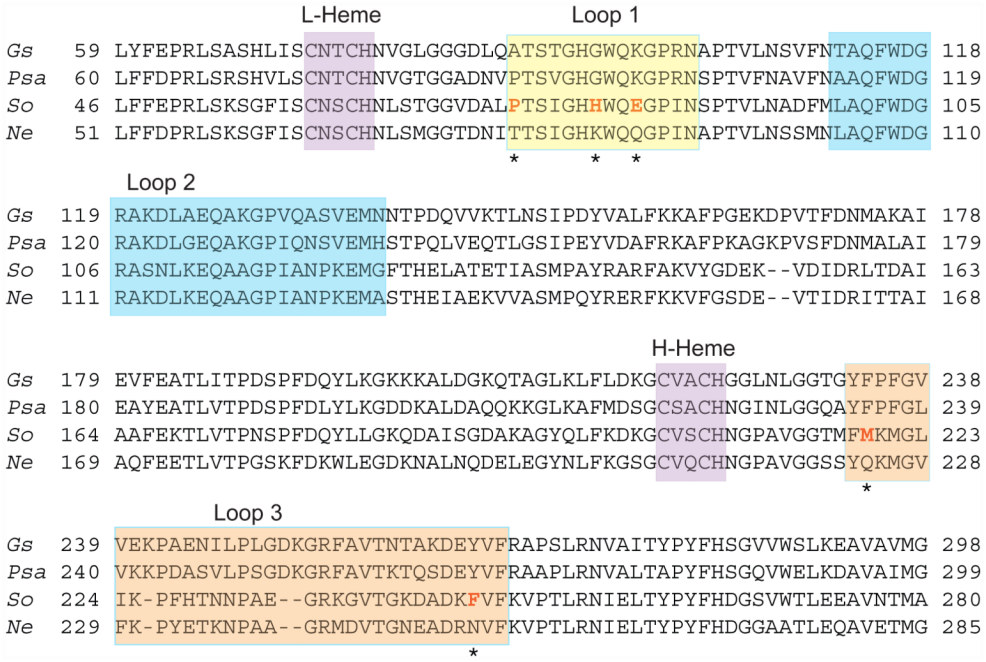

Figure 2.

Partial sequence alignment of various bacterial C*c*Ps. *Gs: Geobacter sulfurreducens*, *Psa: Pseudomonas auruginosa*, *So: Shewanella oneidensis*, *Ne: Nitrosomonas europaea*. Heme binding motifs (CXXCH) are marked with purple shading, and the three loop regions implicated in reductive activation are shaded in yellow, blue or orange.

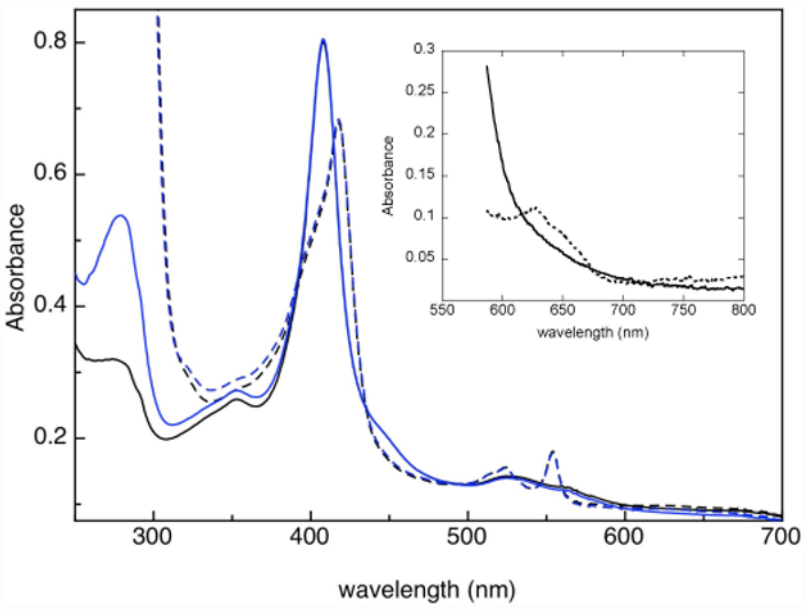

Figure 3.

Electronic absorption spectrum of the oxidized (solid, black) and semi-reduced (dashed, black) tag-free *So* C*c*P, and oxidized (solid, blue) and semi-reduced (dashed, blue) MBP-fusion *So* C*c*P. The inset shows the absorption spectrum of tag-free oxidized and semi-reduced *So* C*c*P at 8 times higher concentration.

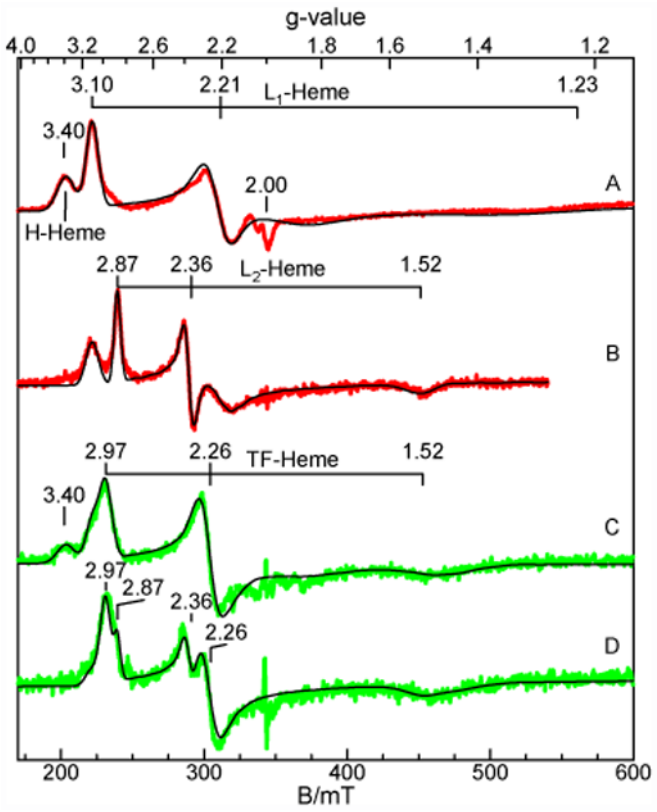

Figure 4.

EPR spectra of 0.5 mM C*c*P in the absence and presence of sodium L-ascorbate with simulations overlaid. (A) *So* C*c*P-MBP, (B) Semi-reduced *So* C*c*P-MBP, (C) tag-free *So* C*c*P, (D) semi-reduced tag-free *So* C*c*P. Experiments were conduced with microwave frequency of 9.62 GHz, power of 0.02 mW, and temperature of 7 K.

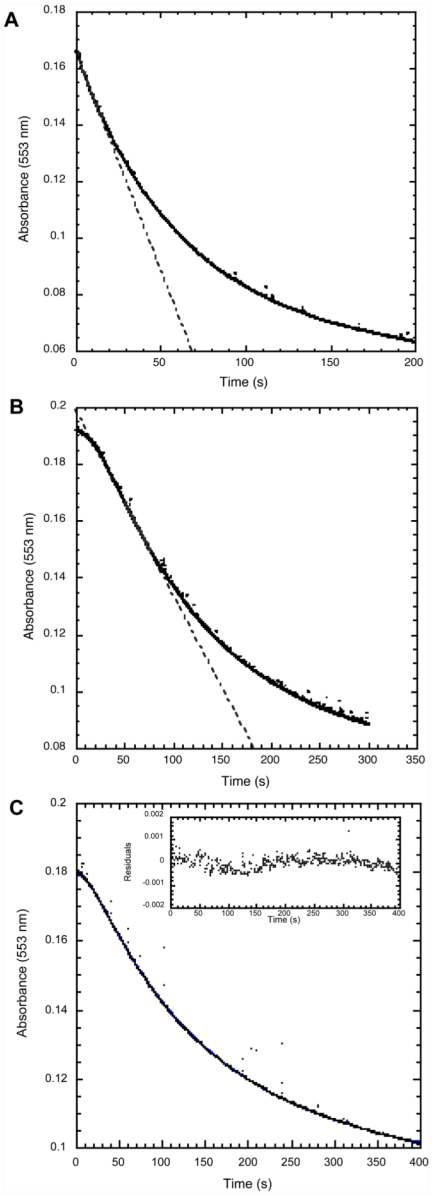

Figure 5.

Comparison of peroxidase catalytic activity using *So* cyt *c*5 (4 μM) as the electron donor for (A) semi-reduced tag-free *So* C*c*P and (B & C) oxidized tag-free *So* C*c*P. Experiments are conducted in 5 mM MES, 5 mM HEPES, 10 mM NaCl, 1 mM $CaCl_2$ (pH 6.0) at 23°C. In A & B, points represent the data and a line represents the linear rate used for Michaelis-Menten analysis. Pane C compares the experimental data (points) to the least-square fit of the data to the kinetic model (line) as described in the text. The inset in (C) shows the residuals of the least-square fit.

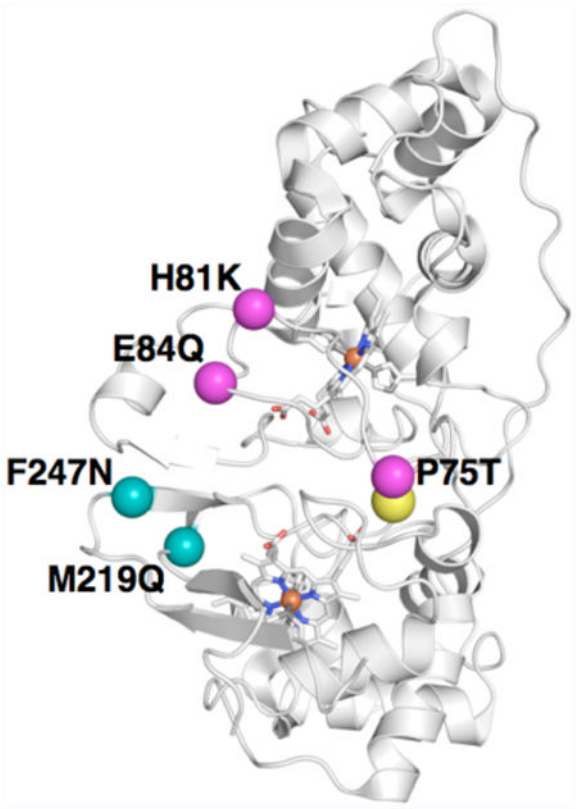

Figure 6.

Depiction of the mutations made in either loop 1 or loop 3 in *So* C*c*P. Using the *Psa* fully oxidized structure as a model, locations of the loop 1 triple mutant P75T/H81K/E85Q are indicated as magenta spheres at the alpha carbon position. The loop 3 double mutant positions M219Q and F247N are shown as teal spheres at the predicted alpha carbon positions.

Table 1

EPR parameters of the C*c*P-MBP and tag-free *So* C*c*P in the oxidized and semi-reduced states.

Heme Species	Amount with respect to total Fe (%)			
	C*c*P-MBP	**Semi-red C*c*P-MBP**	**Tag free C*c*P**	**Semi-red Tag free C*c*P**
H-Heme	50	0	33	0
L_1-Heme	50	34	33	11
L_2-Heme	0	20		8
TF-Heme	0	0	33	33

Table 2

Kinetic parameters of both the oxidized and semi-reduced states of *So* C*c*P-MBP and tag-free *So* C*c*P.

		CcP-MBP		Tag-free CcP	
Electron Donor[†]	**Parameter**[§]	**Semi-red**	**Oxidized**	**Semi-red**	**Oxidized**
Horse heart cyt *c*	K_m (μM) for H_2O_2	0.13 ± 0.08	0.3 ± 0.1	0.03 ± 0.01	0.17 ± 0.05
	k_{cat}^{obs} (s^{-1})	35 ± 3	13 ± 1	1.9 ± 0.2	1.3 ± 1.0
	k_{cat}^{obs}/K_m ($M^{-1}s^{-1}$) ×10^6	280	46	74	7.5
So cyt *c*5	K_m (μM) for H_2O_2	0.1 ± 0.1	0.8 ± 0.1	0.3 ± 0.1	0.6 ± 0.5
	k_{cat}^{obs} (s^{-1})	10 ± 1	0.8 ± 0.1	73 ± 5	7 ± 5
	k_{cat}^{obs}/K_m ($M^{-1}s^{-1}$) ×10^6	100	1	240	12
Azurin	K_m (μM) for H_2O_2	0.2 ± 0.2	0.3 ± 0.1	0.2 ± 0.1	0.4 ± 0.1
	k_{cat}^{obs} (s^{-1})	40 ± 20	12 ± 2	3.4 ± 0.3	1.3 ± 0.1
	k_{cat}^{obs}/K_m ($M^{-1}s^{-1}$) ×10^6	202	38	17	3

[†]Electron donors are horse heart cytochrome *c* (10 μM), *So* cyt *c*5 (4 μM) or azurin (12 μM).

[§]Assays were conducted in 5 mM MES, 5 mM HEPES, 10 mM NaCl, 1 mM $CaCl_2$ (pH 6.0) at 23°C.

Biochemistry. Author manuscript; available in PMC 2013 July 26.

Table 3

Comparison of literature values of the peroxide turnover parameters of various bacterial diheme cytochrome *c* peroxidases in the semi-reduced state using cytochromes *c* as an electron donor.

Organism ‡	K_m (μM) for H_2O_2	k_{cat}^{obs} (s^{-1})	Electron donor (concentration)	k_{cat}^{obs}/[ED] ($s^{-1}\mu M^{-1}$)&	Required Pre-reduction?	Reference
Psa	6	118	*Psa* cyt 551 (13 μM)	14	Yes	(24)
Rc *	33	40	*Rc* cyt *c*2 (18 μM)	2	Yes	(34)
Pss	1.8	88	*Pss* cyt *c*551 (7 μM)	13	Yes	(17)
Gs	6.2	15.5	ABTS (3 mM)		Yes	(18)
Mc	0.5	50	*Mc* cyt *c*555 (9 μM)	5	No	(20)
So	0.3	73	*So* cyt *c*5 (4 μM)	18	Yes	This Study

‡Abbreviations match those used in the text.

*Turnover for as-isolated protein.

&This approximation holds because the concentration of electron donor is much less than the estimated K_M, therefore the rate is approximately linear with electron donor concentration.

Table 4

Model-derived kinetic parameters for peroxidase turnover initiated with oxidized *So* C*c*P.

Electron donor	Peroxidase	Activation rate k_{act} (s^{-1})	Peroxide turnover rate k_1 (s^{-1})*
So cyt *c*5	*So* C*c*P-MBP	0.05 ± 0.01	1.6 ± 0.4
	So C*c*P	0.07 ± 0.02	7 ± 1
Horse heart cyt *c*	*So* C*c*P-MBP	0.08 ± 0.02	1.6 ± 0.4
	So C*c*P	0.02 ± 0.007	0.28 ± 0.08

*Turnover values correspond to 4 μM electron donor, with the K_D for electron donor binding to C*c*P set to 7 μM.

Table 5

Kinetic parameters of both the oxidized and semi-reduced states of tag-free *So* C*c*P variants using *So c*5 as the electron donor.

			K_m for H_2O_2 (μM)	k_{cat}^{obs} (s^{-1})	k_{act} (s^{-1})	k_1 (s^{-1})*
Loop 1	P75T/H81K/E84Q	Oxidized	1.0 ± 0.3	0.3 ± 0.1	0.6 ± 0.2	0.56± 0.04
		Semi-reduced	0.4 ± 0.3	13 ± 1	n.a.	n.a.
Loop 3	M219Q/F247N	Oxidized	1.6 ± 0.2	0.5 ± 0.1	0.09 ± 0.01	0.60 ± 0.04
		Semi-reduced	0.5 ± 0.3	5.9 ± 0.5	n.a.	n.a.
Wild type		Oxidized	0.6 ± 0.5	7 ± 5	0.07 ± 0.02	7 ± 1
		Semi-reduced	0.3 ± 0.1	73 ± 5	n.a.	n.a.

*Turnover values correspond to 4 μM electron donor.